Aalborg Universitet

AALBORG UNIVERSITY

DC protection criteria for multi-terminal HVDC system considering transient stability of embedded AC grid

Niaki, Seyed Hassan Ashrafi; Chen, Zhe; Bak-Jensen, Birgitte; Sharifabadi, Kamran; Liu, Zhou; Hu, Shuju

Published in:
International Journal of Electrical Power & Energy Systems

DOI (link to publication from Publisher):
10.1016/j.ijepes.2024.109815

Creative Commons License
CC BY-NC-ND 4.0

Publication date:
2024

Document Version
Publisher's PDF, also known as Version of record

Link to publication from Aalborg University

Citation for published version (APA):
Niaki, S. H. A., Chen, Z., Bak-Jensen, B., Sharifabadi, K., Liu, Z., & Hu, S. (2024). DC protection criteria for multi-terminal HVDC system considering transient stability of embedded AC grid. *International Journal of Electrical Power & Energy Systems*, *157*, Article 109815. https://doi.org/10.1016/j.ijepes.2024.109815

General rights
Copyright and moral rights for the publications made accessible in the public portal are retained by the authors and/or other copyright owners and it is a condition of accessing publications that users recognise and abide by the legal requirements associated with these rights.

- Users may download and print one copy of any publication from the public portal for the purpose of private study or research.
- You may not further distribute the material or use it for any profit-making activity or commercial gain
- You may freely distribute the URL identifying the publication in the public portal -

Take down policy
If you believe that this document breaches copyright please contact us at vbn@aub.aau.dk providing details, and we will remove access to the work immediately and investigate your claim.

Downloaded from vbn.aau.dk on: July 04, 2025

Electrical Power and Energy Systems 157 (2024) 109815

Contents lists available at ScienceDirect

International Journal of Electrical Power and Energy Systems

journal homepage: www.elsevier.com/locate/ijepes

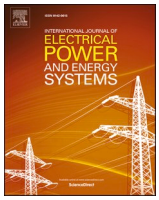

DC protection criteria for multi-terminal HVDC system considering transient stability of embedded AC grid

Seyed Hassan Ashrafi Niaki [a,*], Zhe Chen [a], Birgitte Bak-Jensen [a], Kamran Sharifabadi [b], Zhou Liu [c], Shuju Hu [d]

[a] Department of Energy Technology, Aalborg University, Denmark
[b] Equinor ASA, Fornebu, Norway
[c] Siemens Gamesa Renewable Energy A/S, Denmark
[d] Chinese Academy of Sciences, China

ARTICLE INFO

Keywords:
VSC-HVDC system
Multi-terminal HVDC grid
HVDC protection
HVDC stability
DC fault

ABSTRACT

To build up a secure AC/DC power grid, a reliable DC protection system is vital for multi-terminal HVDC systems. However, efficient and reliable DC protection has always been a major challenge. On the other side, the characteristics of the embedded AC grid have a mutual impact on transient interactions with HVDC system dynamics and protection. The whole AC/DC grid including the HVDC system and the embedded AC grid must remain stable after a severe disturbance i.e., DC fault. Thus, the DC protection should be designed in a way that not only is reliable but also fast enough to prevent system instability, especially in the case of a weak embedded AC grid. However, there has been a lack of research on how fast DC protection should be regarding the transient stability of the embedded AC grid. This study presents a novel survey into DC protection criteria of the multi-terminal HVDC systems regarding the transient stability of the embedded AC grid. The study analytically investigates the effects of different grid parameters including HVDC power, converter transformer reactance and arm reactor on system security. Then, the discussion has been extended to discuss DC protection criteria, e.g., required speed, for the multi-terminal HVDC systems. A variety of simulations have been tested in the PSCAD platform using a multi-terminal HVDC case study. The outcomes can be used for the protection study of the multi-terminal HVDC systems and the selection of appropriate CBs.

1. Introduction

HVDC system is a favorable option for transmitting bulk power through long-distance routes, e.g., remote offshore wind farms [1]. Voltage Source Converter (VSC) based HVDC technology provides power systems with independent control of active and reactive powers [2]. VSC-HVDC system is a feasible solution for connecting more than two DC terminals to create a multi-terminal HVDC grid [3]. The multi-terminal VSC-HVDC grid plays a major role in having a secure and stable power system and integrating large-scale renewable energy sources [4]. DC faults are more severe than AC ones, as there is low impedance on the DC side compared to the AC side [5]. Therefore, there have been many studies on DC protection regarding fault detection and fault-handling strategies for multi-terminal HVDC systems [6,7]. Most of the presented studies have used the traveling-wave theory or frequency-domain analysis for DC fault detection [8,9]. Also, some studies have been proposed to make a better coordination between HVDC converters and DC Circuit Breakers (DCCB) [10]. On the other hand, such a large disturbance as a DC fault can easily threaten the system's transient stability [11]. Consequently, the DC protection and stability of the multi-terminal VSC-HVDC grid should be considered simultaneously. Although, there are lots of studies on the DC protection of the multi-terminal VSC-HVDC systems [12,13], the transient stability issues are not considered normally in the design of the DC protection. It is necessary to keep the stability of the VSC-HVDC system under DC fault conditions. Thus, DC protection should be designed so that the system is capable of being stable after DC fault clearance. On the other hand, grid characteristics like Short Circuit Ratio (SCR) have a considerable effect on AC/DC system stability [14]. Consequently, such grid characteristics affect the design of the DC protection system for the multi-terminal VSC-HVDC networks.

Based on the author's knowledge, there are not enough studies on how to select an appropriate protection system for the multi-terminal

* Corresponding author.
E-mail address: shani@et.aau.dk (S. Hassan Ashrafi Niaki).

https://doi.org/10.1016/j.ijepes.2024.109815
Received 12 April 2023; Received in revised form 9 August 2023; Accepted 18 January 2024
Available online 29 January 2024
0142-0615/© 2024 The Author(s). Published by Elsevier Ltd. This is an open access article under the CC BY-NC-ND license (http://creativecommons.org/licenses/by-nc-nd/4.0/).

Nomenclature

FDT_i	Fault detection time of DC link i.
FIT_i	Fault interruption time of protection system for DC link i.
FIT_{ip}	Fault interruption time of primary protection for DC link i.
FIT_{ib}	Fault interruption time of backup protection for DC link i.
CCT_i	Critical clearing time for fault at DC link i.
CDT_i	Communication delay time for backup protection activation of DC link i.
SCC	Short circuit capacity.
SCR	Short circuit ratio.
P_{HVDC}	HVDC power value.
V_S,V_{PCC}	AC equivalent source and PCC point voltages.
Z_{SC}	Short circuit impedance of the AC source.
P_{PCC},Q_{PCC}	Active and reactive power at PCC point.
P_m,P_{LOSS}	Mechanical power and HVDC converter power loss.
f_s	Power system frequency.
H	Inertia time constant.
$\delta\delta_{cr}$,δ_0	Electrical, critical, initial load angles.
X_{SC}	Short circuit reactance of AC source.
X_T	Reactance of HVDC converter transformer.
L_{DC},L_{Arm}	DC and arm inductances.
R_{DC},R_{Arm}	DC and arm resistances.
R_{eq},L_{eq}	Equivalent resistance and inductance on DC side after fault occurrence at DC terminal.
V_{VSC}	Voltage at AC terminal of VSC converter.
P_{VSC}	Power at AC terminal of VSC converter.
V_{DC}	Nominal HVDC voltage.
V_{DCC}^{-},V_{DCC}^{+}	DC voltage before DC reactors, before and after DC fault instant.
V_{DC}^{-},V_{DC}^{+}	DC voltage after DC reactors, before and after DC fault instant.
I_f,I_{PCC}	DC fault and PCC point currents.
m	Modulation index.
k_{SF}	Safety factor value.

VSC-HVDC grids considering the grid characteristics of the embedded AC grid. AC-side grid characteristics including SCR and inertia time constant are influential on the system dynamics [15]. DC-side grid dynamics are not independent of AC-side dynamics. Therefore, DC-side stability and AC-side stability are intertwined [16]. Consequently, the AC-side grid characteristics can affect HVDC system stability under large disturbances. On the other hand, DC-side grid characteristics including HVDC power and DC reactor have a considerable impact on HVDC dynamics. Therefore, each specific multi-terminal VSC-HVDC grid should end up with a unique DC protection based on its own characteristics including the parameters of the embedded AC grid. But the fastest DC protection via the fastest DCCBs is usually recommenced in the literature, regardless of the characteristics of the embedded AC grid [17,18]. However, the faster DCCB to interrupt faults can incur higher capital costs [19]. Although faster DC protection leads to a higher safety margin, it can be too expensive and not economical for some HVDC grids which do not need the faster DC protection. On the contrary, using slow DCCBs may threaten the stability of some other multi-terminal HVDC systems. Therefore, one of this study's goals is to determine the minimum required speed of the DC protection system considering the transient stability and the characteristics of the embedded AC grid. In other words, the study sheds light on a trade-off between the cost and technical adequacy in selecting DC protection and types of DCCBs.

For the first time, this study discusses the appropriate selection of DC protection considering the transient stability of the embedded AC grid for the multi-terminal VSC-HVDC systems. Appropriate action time for the DC protection system to prevent the system's transient instability has been discussed in the paper. The study also investigates the effects of the grid characteristics including AC-side and DC-side ones on the stability of the VSC-HVDC systems. In addition, the impact of the arm reactor in the HVDC converter is discussed in this paper. Analytic relations based on different grid parameters are presented to demonstrate their impact on the system's security and stability. Then, appropriate CBs are selected considering the transient stability margin under DC fault conditions.

This paper is organized as follows: grid characteristics and definitions related to combined AC/DC power systems are presented in Section 2. Section 3 discusses the effects of different grid characteristics on the VSC-HVDC system stability and protection. HVDC case study and simulation results are presented in Section 4. Finally, conclusions are drawn in Section 5.

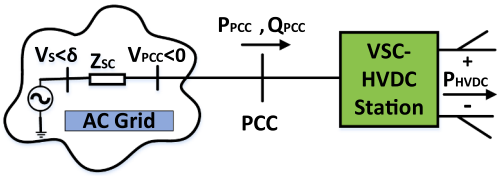

Fig. 1. a VSC-HVDC system connected to an AC power grid at a PCC point.

2. Grid characteristics and definitions for combined AC/DC power system

Fig. 1 shows a VSC-HVDC system connected to an AC power source, based on synchronous machine model, at the Point of Common Coupling (PCC). The HVDC system may have multiple DC terminals as shown in Fig. 1. For this system, Short Circuit Ratio (SCR) is equal to the Short Circuit Capacity (SCC) divided by the amount of HVDC power [20]. The SCC and the SCR definitions for an AC grid connected to an HVDC system are as follow:

$$SCR = \frac{SCC_{MVA}}{P_{HVDC}} = \frac{V_S^2}{P_{HVDC} Z_{SC}} \tag{1}$$

Where Z_{SC} is the short circuit impedance of the AC power system. Mechanical and electrical power difference can be calculated based on electrical load angle as follow:

$$P_m - P_{PCC} = \frac{2H}{(2\pi f_s)} \frac{d^2\delta}{dt^2} \tag{2}$$

Where H is the inertia time constant of the synchronous machine. The electrical active power at the PCC point can be achieved as follows [20]:

$$P_{PCC} = \frac{V_S \times V_{PCC}}{X_{SC}} \sin(\delta) \tag{3}$$

Where X_{SC} is the short circuit reactance of the AC power system. The power at the PPC point consists of the HVDC power and the power loss of the VSC-HVDC station.

$$P_{PCC} = P_{HVDC} + P_{loss} \tag{4}$$

The power losses include the HVDC converter loss and converter transformer loss which are negligible compared to the HVDC power. Therefore, the HVDC power value is almost equal to the power at the PCC point:

$$P_{PCC} = P_{HVDC} \tag{5}$$

Consequently, using (3) and (5), the following relation can be achieved:

$$P_{HVDC} = \frac{V_S \times V_{PCC}}{X_{SC}} \sin(\delta) \tag{6}$$

Equation (6) describes the relationship between the load angle of the AC power grid and the HVDC power value. As the HVDC power value increases, the load angle goes up. Thus, the stability margin decreases with an increase in the HVDC power. Generally, electrical power systems can be categorized into three groups based on the grid strength, the SCR value [20]:

- Strong grid: the grids with SCR > 3
- Weak grid: the grids with $2 <$ SCR < 3
- Very weak grid: the grids with SCR < 2

Using (1) and (6), the relation between the SCR and the load angle can be expressed as follow:

$$P_{HVDC} = \frac{V_S^2}{SCR \times Z_{SC}} = \frac{V_S \times V_{PCC}}{X_{SC}} \sin(\delta) \tag{7}$$

If the SCR value increases, the load angle decreases. Therefore, the grid strength and the HVDC power value are influential parameters on the transient stability of the AC/DC power system including the VSC-HVDC grids. This section's discussion was based on the well-known model of single-machine infinite bus system for the transient stability analysis [20]. In this section, the system is developed to consider the impact of the HVDC connection on the grid dynamics. This primary discussion is the background for further development in the next section. Although the discussed model is based on a single HVDC system, it is valid and extendable to multi-terminal HVDC systems. As an HVDC system usually isolates one AC grid from another AC grid, dynamic effect of an AC grid on another remote AC grid in the multi-terminal HVDC grid can be ignorable. Therefore, each area of a multi-terminal HVDC system i.e. an AC grid connected to an HVDC station can be investigated separately. On the other hand, the VSC converters are usually blocked under DC fault conditions. Consequently, the impact of the converter control is limited on the system transient behavior under DC fault conditions. Thus, the proposed background is used for further investigation in the next section.

3. Effect of grid characteristics on VSC-HVDC system stability and protection

The VSC-HVDC system stability depends on grid characteristics and parameters both on AC and DC sides. Therefore, it is necessary to investigate the system's transient stability under DC fault conditions considering the grid characteristics. On the other hand, the protection system of a VSC-HVDC grid should secure the network against different DC pole faults. DC protection system should be fast enough so that the HVDC system successfully recovers to normal operation as soon as possible after fault clearance. An ineffective protection system may lead to system instability during and after DC fault conditions. This section investigates the impacts of the AC/DC grid characteristics on the transient stability of the VSC-HVDC system. Due to a large number of grid parameters, different parameter pairs are selected in this survey. Also, the DC protection design of the VSC-HVDC grid considering the system transient stability is proposed in the last sub-section.

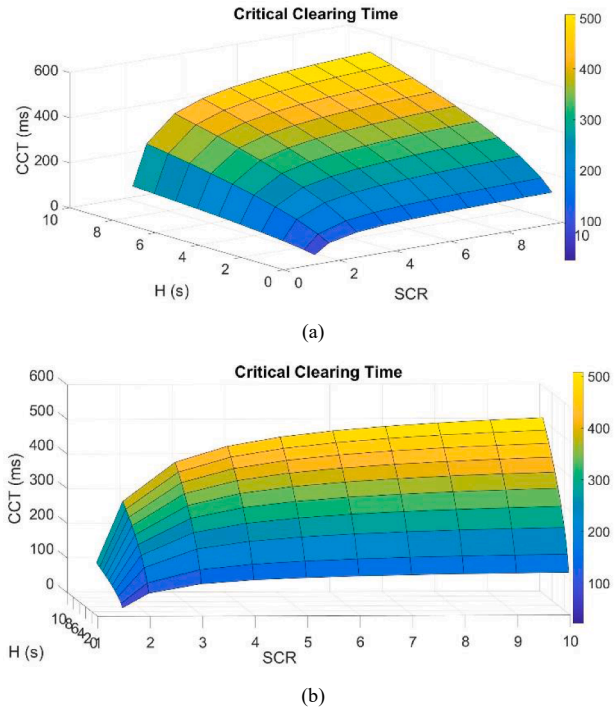

Fig. 2. CCT based on different SCR and H values, (a) perspective a, (b) perspective b.

3.1. Impact of AC-side grid characteristics on VSC-HVDC system stability

DC faults in an HVDC system can remarkably affect voltage and current values on both the DC and AC sides of an AC/DC grid [21]. The AC-side grid characteristics including SCR and inertia time constant can considerably influence the transient stability of the AC grid [14]. Moreover, the reactance of the converter transformer can be influential on the system's transient stability. As the system stability of AC/DC power grids is united, these grid parameters can affect the HVDC system stability too. Therefore, the system stability margin of a VSC-HVDC system connected to a strong AC grid is different from the one connected to a weak AC grid. Consequently, the DC protection design for these two cases will be different. Critical Clearing Time (CCT) is the maximum time to clear a fault without losing the system stability [20]. A power grid can keep its stability if the fault is cleared before the CCT time. In this part, the impacts of the following parameter pairs on the CCT value are analyzed:

- SCR and H.
- XT and H.

The CCT can be calculated based on the initial and critical load angles as follows [22]:

$$CCT = \sqrt{\frac{2H(\delta_{cr} - \delta_0)}{\pi f_s P_m}} \tag{8}$$

$$\delta_{cr} = \cos^{-1}((\pi - 2\delta_0)\sin(\delta_0) - \cos(\delta_0)) \tag{9}$$

If $Z_{SC} \approx X_{SC}$, the following relation can be achieved from (9):

$$\delta_0 = \sin^{-1}\left(\frac{V_S}{V_{PCC} SCR}\right) \tag{10}$$

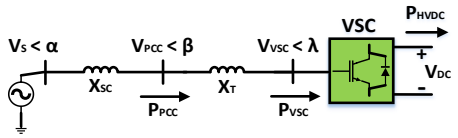

Fig. 3. a VSC-HVDC system connected to an AC power grid considering the reactance of the converter transformer.

relation between the CCT value and the transformer reactance. It can be seen from two perspectives of Fig. 4 that the CCT value decreases when the XT value increases. Although the XT parameter is not as effective as the SCR parameter, a change from 0.1 to 0.2p.u. for this parameter causes about a 20 % decrease in the CCT value, as shown in Fig. 4 (b). Therefore, selecting the converter transformers with smaller reactance can improve the system transient stability including the VSC-HVDC stability. Also, for some transformer designs, grounding reactance may be unified with the main transformer. This may affect the equivalent reactance of the transformer.

$$CCT(SCR,H)=\sqrt{\frac{2H\left(\cos^{-1}\left(\frac{\pi V_S}{V_{PCC}SCR}-\sin^{-1}\left(\frac{V_S}{V_{PCC}SCR}\right)\frac{2V_S}{V_{PCC}SCR}-\sqrt{1-\frac{V_S^2}{V_{PCC}^2SCR^2}}\right)-\sin^{-1}\left(\frac{V_S}{V_{PCC}SCR}\right)\right)}{\pi f_s P_m}} \tag{11}$$

Using (8), (9) and (10), the CCT can be calculated based on the AC grid parameters SCR and H as in (11). To have an efficient analysis, equation (11) is implemented in the MATLAB platform and the results are presented in 3D illustrations. The CCT values corresponding to the SCR values with different inertia time constants are shown in Fig. 2. It is clear from two perspectives of Fig. 2 that the CCT value rises when the SCR and H values increase. The sensitivity of the CCT values to SCR for weak grids (lower SCRs) is higher than the ones for strong grids (higher SCRs), as shown in Fig. 2 (b).

To analyze the impact of the converter transformer reactance, the equivalent circuit of the system is presented in Fig. 3 in more detail. Converter transformer loss and VSC converter loss are ignorable. Like (6), the following relations can be achieved for this system:

$$P_{PCC}=\frac{V_S\times V_{VSC}}{(X_T+X_{SC})}\sin(\alpha-\lambda) \tag{12}$$

$$P_{PCC}=P_{VSC}=P_{HVDC}\delta=\alpha-\lambda \tag{13}$$

Then:

$$V_{VSC}=\sqrt{V_{PCC}^2-X_T^2I_{PCC}^2} \tag{14}$$

$$P_{HVDC}=\frac{V_S\times V_{VSC}}{(X_T+X_{SC})}\sin(\delta) \tag{15}$$

Using (14) and (15), the following equation can be calculated:

$$\delta_0=\sin^{-1}\left(\frac{P_{HVDC}\times(X_T+X_{SC})}{V_S\times V_{VSC}}\right)=\sin^{-1}\left(\frac{P_{HVDC}\times(X_T+X_{SC})}{V_S\times\sqrt{V_{PCC}^2-X_T^2I_{PCC}^2}}\right) \tag{16}$$

3.2. Impact of DC-side grid characteristics on VSC-HVDC system stability

On the DC side, there are two important parameters of the DC reactor and arm reactor to be investigated for the transient stability studies. In addition, HVDC power is an influential parameter on the VSC-HVDC stability. Thus, the following parameter pairs are selected to analyze in this part:

- L_{DC} and P_{HVDC}.
- L_{Arm} and P_{HVDC}.

The equivalent circuit of the system considering DC reactors are depicted in Fig. 5. Under normal operation condition, the voltage drop through the DC reactors is almost zero. In the other word, DC voltages before and after DC reactors at the instant before the DC fault happening are almost the same and equal to the nominal HVDC voltage:

$$V_{DCC}^{-}=V_{DC}^{-}=V_{DC} \tag{18}$$

On the other hand, the voltage at the AC terminal of the VSC converter, i.e. the secondary side of the converter transformer can be calculated as follows [23]:

$$V_{VSC}^{-}=\frac{\sqrt{3}}{2\sqrt{2}}mV_{DCC}^{-}=\frac{\sqrt{3}}{2\sqrt{2}}mV_{DC} \tag{19}$$

Where m is the modulation index of the VSC-HVDC converter. Modular Multilevel Converter (MMC) is a popular type of power converter for the VSC-HVDC grids.

Suppose that a DC fault happens at the beginning of the DC link as shown in Fig. 5. When a DC fault occurs, the MMC converter will be blocked and anti-parallel diodes of the power semiconductors in each module start feeding the fault current [24]. Fig. 6 (a) depicts the schematic of an MMC with an arm reactor in each arm of the converter under DC fault conditions. As shown in Fig. 6 (b), the MMC modules are blocked and the fault current passes through anti-parallel diodes. The equivalent circuit of the system under the DC fault condition is depicted

$$CCT(X_T,H)=\sqrt{\frac{2H\left(\cos^{-1}\left(\frac{\pi P_{HVDC}(X_T+X_{SC})}{V_S\sqrt{V_{PCC}^2-X_T^2I_{PCC}^2}}-\sin^{-1}\left(\frac{P_{HVDC}(X_T+X_{SC})}{V_S\sqrt{V_{PCC}^2-X_T^2I_{PCC}^2}}\right)\frac{2P_{HVDC}(X_T+X_{SC})}{V_S\sqrt{V_{PCC}^2-X_T^2I_{PCC}^2}}-\sqrt{1-\frac{P_{HVDC}^2(X_T+X_{SC})^2}{V_S^2(V_{PCC}^2-X_T^2I_{PCC}^2)}}\right)-\sin^{-1}\left(\frac{P_{HVDC}(X_T+X_{SC})}{V_S\sqrt{V_{PCC}^2-X_T^2I_{PCC}^2}}\right)\right)}{\pi f_s P_m}} \tag{17}$$

Thus, using (8), (9) and (16), the CCT can be achieved based on the equivalent reactance of the converter transformer as in (17). The reactance of the converter transformer is usually in the range of 0.1 to 0.2p.u. Therefore, this range is selected for the analysis. Fig. 4 shows the

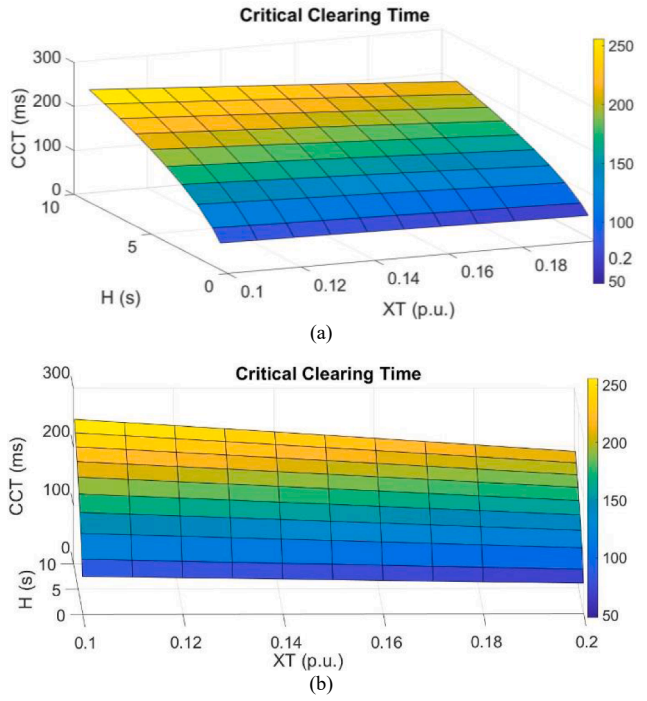

Fig. 4. CCT based on different XT and H values, (a) perspective a, (b) perspective b.

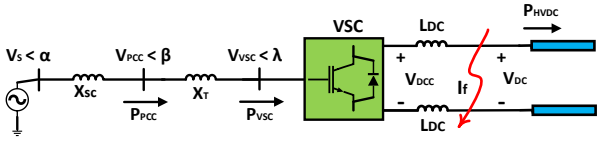

Fig. 5. a VSC-HVDC system connected to an AC grid with DC reactors.

in Fig. 6 (c). After the DC fault happening, the DC voltage at the beginning of the DC link V_{DC}^{+}, will be zero. Considering Fig. 6 (c), the following relations can be achieved under the DC fault condition:

$$R_{eq} = \frac{2}{3}R_{arm} + 2R_{DC} \tag{20}$$

$$L_{eq} = \frac{2}{3}L_{arm} + 2L_{DC} \tag{21}$$

$$R_{eq}I_f + L_{eq}\frac{dI_f}{dt} = V_{DC}^{-} - V_{DC}^{+} = V_{DC} - 0 = V_{DC} \tag{22}$$

The equivalent resistance is ignorable. Then, using (21) and (22):

$$\frac{dI_f}{dt} = \frac{V_{DC}}{L_{eq}} = \frac{V_{DC}}{\frac{2}{3}L_{arm} + 2L_{DC}} \tag{23}$$

Considering Fig. 5, the following equation can be expressed:

$$V_{DC}^{+} = V_{DCC}^{+} - 2L_{DC}\frac{dI_f}{dt} = 0 \tag{24}$$

Using (23), (24) and (19), the following equations can be calculated:

$$V_{DCC}^{+} = \frac{2L_{DC}V_{DC}}{\frac{2}{3}L_{arm} + 2L_{DC}} \tag{25}$$

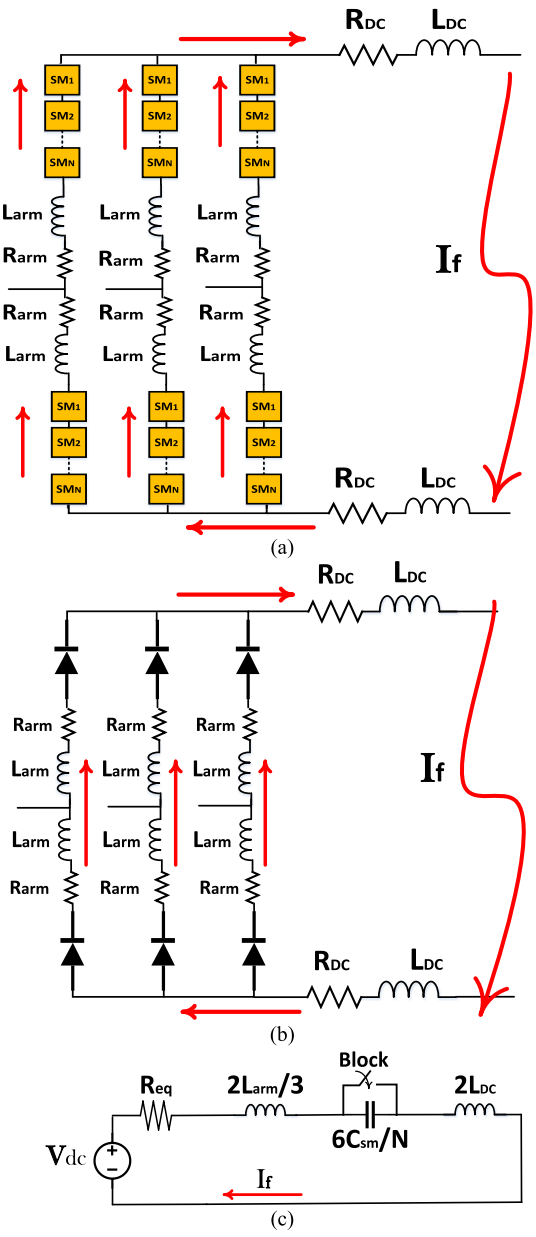

Fig. 6. MMC-HVDC system under DC fault condition, (a) MMC structure, (b) anti-parallel diode feeding, (c) the equivalent circuit.

$$V_{VSC}^{+} = \frac{\sqrt{3}}{2\sqrt{2}}mV_{DCC}^{+} = \frac{\sqrt{3}}{2\sqrt{2}}m\left(\frac{2L_{DC}}{2/3L_{arm} + 2L_{DC}}\right)V_{DC} \tag{26}$$

The initial load angle can be achieved based on (16) and (26) as follow:

$$\delta_0 = \sin^{-1}\left(\frac{2\sqrt{2}}{\sqrt{3}}\left(\frac{2/3L_{arm} + 2L_{DC}}{2L_{DC}}\right)\frac{P_{HVDC}(X_T + X_{SC})}{mV_SV_{DC}}\right) \tag{27}$$

To avoid too long formulation for the CCT, it is supposed that:

$$K = \frac{2\sqrt{2}}{\sqrt{3}}\frac{(X_T + X_{SC})}{mV_SV_{DC}} \tag{28}$$

$$CCT(L_{DC}, P_{HVDC}) = CCT(L_{arm}, P_{HVDC}) = \sqrt{\frac{2H\left(\cos^{-1}\left(\left(\pi - 2\sin^{-1}\left(\frac{(2/3L_{arm}+2L_{DC})P_{HVDC}}{2L_{DC}}K\right)\right)\left(\frac{(2/3L_{arm}+2L_{DC})P_{HVDC}}{2L_{DC}}K\right) - \sqrt{1-\left(\frac{(2/3L_{arm}+2L_{DC})P_{HVDC}}{2L_{DC}}K\right)^2}\right) - \sin^{-1}\left(\frac{(2/3L_{arm}+2L_{DC})P_{HVDC}}{2L_{DC}}K\right)\right)}{\pi f_s P_m}} \quad (29)$$

Finally, the relation for the CCT calculation based on the DC and arm reactors is expressed in (29). The CCT values based on L_{DC} and P_{HVDC} parameters are depicted in Fig. 7. The HVDC power value is in the range of 0.5p.u. to 1.4p.u. Also, the DC reactor value changes from 0.01p.u. to 0.2p.u. It can be seen from Fig. 7 (a) that the CCT remarkably decreases when the HVDC power value increases. On the other hand, CCT rises with an increase in the DC reactor value. Consequently, the system's transient stability improves with larger DC reactors. However, the CCT sensitivity to the changes in the HVDC power is much higher than the change in DC reactor value.

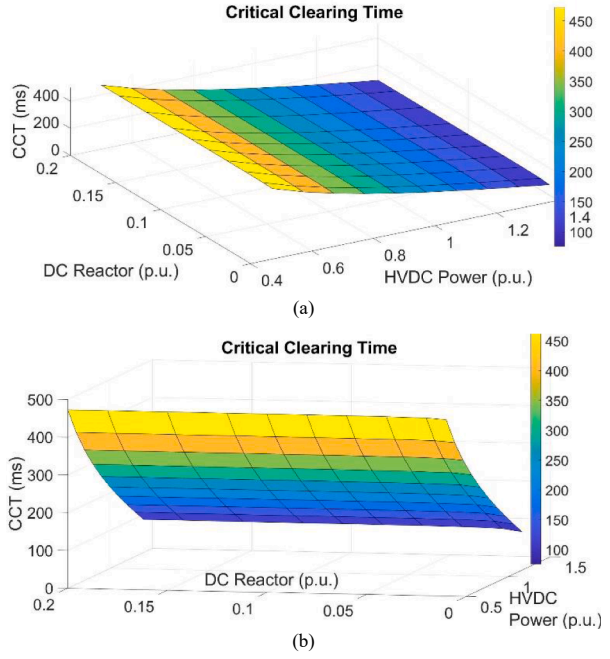

Fig. 7. CCT based on different L_{DC} and P_{HVDC} values, (a) perspective a, (b) perspective b.

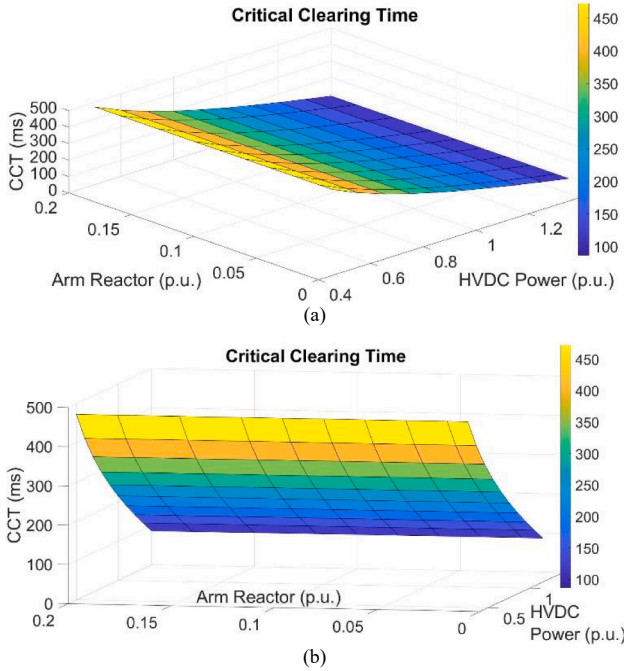

Fig. 8. CCT based on different L_{Arm} and P_{HVDC} values, (a) perspective a, (b) perspective b.

The CCT values based on L_{Arm} and P_{HVDC} parameters are shown in Fig. 8. The arm reactor value changes from 0.01p.u. to 0.2p.u. The CCT slightly decreases with an increase in the arm reactor value. As a result, the transient stability margin reduces with larger arm reactors. However, the CCT sensitivity to the change in the arm reactor is lower than its sensitivity to the change in the DC reactor.

3.3. DC protection design of VSC-HVDC grid considering system transient stability

An effective DC protection must secure the AC/DC grid including the HVDC network against the system instability under DC fault conditions. Therefore, the time duration of the DC protection system including fault detection time and fault interruption time has to be less than the CCT value. Thus, the following relation must be met for DC protection of the multi-terminal VSC-HVDC grid when a fault happens at the DC link i:

$$\underbrace{(FDT_i + FIT_i)}_{protectiontime} < CCT_i \tag{30}$$

To have a more practical approach to selecting an appropriate protection time, unpredictable delays can be considered into (30). The unpredictable delays can be reflected in the relation via a safety factor. Then, protection time considering transient system stability can be calculated as follow:

$$\underbrace{(FDT_i + FIT_i)}_{protectiontime} \leq k_{SF} \times CCT_i 0.7 \leq k_{SF} \leq 1 \tag{31}$$

In addition, a more conservative way of designing DC protection is to consider backup protection into (31):

$$\underbrace{(FDT_i + FIT_{ip})}_{primaryprotectiontime} + \underbrace{(CDT_i + FIT_{ib})}_{backupprotectiontime} < k_{SF} \times CCT_i \tag{32}$$

Fault detection time for VSC-HVDC system is commonly within several milliseconds [13]. Also, communication delay to activate backup protection can take about several milliseconds [25]. On the other hand, fault interruption time is dependent on fault interruption methods that can be categorized into two schemes as follows [17]:

4. Non-selective scheme

4.1. Fully-selective scheme

In a non-selective scheme, the whole HVDC grid will be shut down under DC fault conditions. The DC fault is cleared by the converter's ACCBs. However, for the HVDC grids that share remarkable power with the AC/DC grid, it can threaten the system's security and stability [26]. In addition, it is not suitable for the multi-terminal VSC-HVDC grids, as the whole HVDC grid will collapse. Therefore, it is vital to apply a fully-selective scheme to keep continuous power delivery to consumers under DC fault conditions. In the multi-terminal VSC-HVDC systems with a fully-selective protection scheme, the DCCBs are installed at both ends of each DC link [17]. Consequently, only faulted link is isolated in this scheme through the DCCBs opening assigned to this link.

In general, fault interruption by the DCCBs can be achieved within ten milliseconds [27]. However, there are different types of the DCCBs with different operation times and fault-clearing capabilities [19]. For the VSC-HVDC grid connected to a weak and very weak AC grid, it is necessary to use fast CBs to interrupt the DC fault. Depending on strength of the AC grid, the first scheme of DC protection may not be applicable as ACCBs are not fast enough to clear the fault before CCT time. Thus, the DCCBs are usually needed to interrupt faults for AC grids with low SCR. Moreover, it is necessary to have a fully-selective protection for the multi-terminal VSC-HVDC grids to isolate faulted DC links. In the fully-selective protection scheme, the DCCBs should be selected considering their opening times and the presented relations (30) to (32). Mechanical DCCBs (MD) may not be an appropriate solution for a very short CCT and faster ones like Hybrid DCCBs (HD) should be chosen. Therefore, a unique DC protection including a protection scheme and CB selection is needed for each case of the multi-terminal VSC-HVDC grids considering the system's transient stability.

5. Multi-Terminal VSC-HVDC test system and simulation results

A case study of a four-terminal MMC-HVDC grid is performed in PSCAD as depicted in Fig. 9. The Half-Bridge (HB) MMCs that are used in the case study, are capable of being blocked during fault circumstances. They are usually blocked under DC fault conditions. They can automatically be deblocked after fault clearance. The nominal HVDC voltage is ± 320 kV and the system configuration is a symmetric monopole [28]. The MMC1&2 are connected to offshore wind parks and the MMC3&4

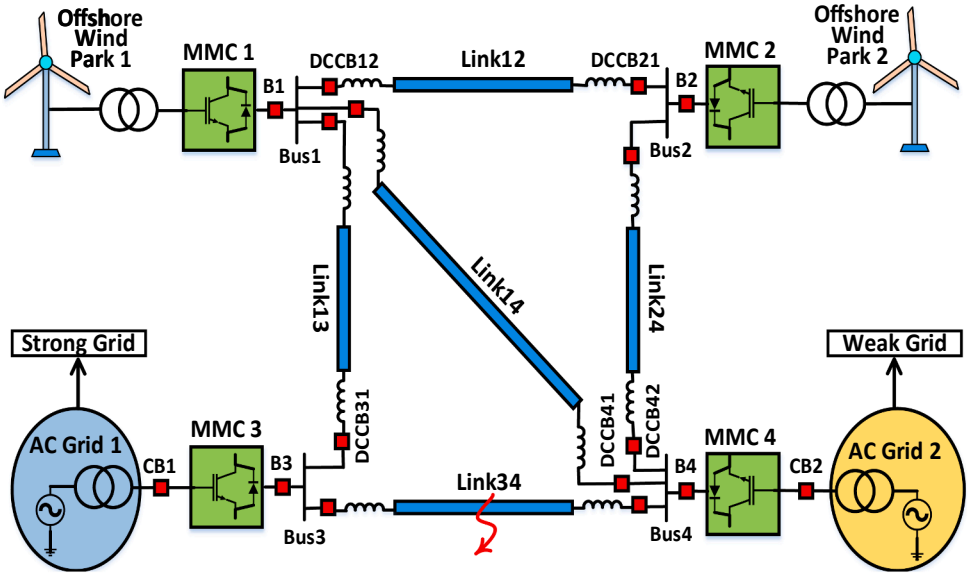

Fig. 9. The case study: a four-terminal MMC-HVDC grid.

are integrated into AC main grids. AC grid 1 and 2 are simulated based on the synchronous machine model. While the rated power of the MMC4 is 1200 MW, the rest of the MMCs have a rated power of 900 MW. To achieve fully-selective protection, DCCBs are installed at both ends of each HVDC link. The lengths of link34, link13&14 and the link12&24 are 400 km and 300 km respectively. The HVDC links are XLPE cables simulated based on a frequency-dependent model. More details of the HVDC case study including the converter modeling and other components can be found in [28].

For DC voltage control of the HVDC case study, droop control is applied to have a higher reliability of the HVDC grid [28]. The MMC3&4 are assigned to control the DC voltage. On the other hand, the MMC1&2 which are connected to offshore wind parks are set to control the active power. For the MMC protection, overcurrent protection is applied to prevent damage to the power semiconductors. The maximum instantaneous threshold for the current of the power semiconductors is typically twice the maximum continuous current [28]. The MMC will be blocked if the current of the power semiconductor exceeds the defined threshold. In addition, undervoltage protection is applied as the MMC controllability is lost if arm voltage becomes too low [28]. Typical values of the DC protection parameters used for the HVDC test system are presented in Table 1. Based on the transient stability margin of the system under DC fault conditions, a suitable DC protection can be chosen for the VSC-HVDC grid.

5.1. The first case Study: Test results for the HVDC grid connected to strong AC grids

As can be seen from Fig. 9, one of the AC grids, AC grid 1, is considered to be a strong grid and AC grid 2 is considered to be a weak grid. Then, by changing the SCR value of the AC grid 2, different case studies are tested. However, for the first case study, both AC grids including the AC grid 1 and 2 are supposed to be strong grids with the SCR = 5. The simulation results for this case are shown in Fig. 10 and Fig. 11, for a Pole-to-Pole (PP) fault happening at the beginning of the link 34 at time 2 s. Measured DC voltages of all buses when the fault is cleared by the mechanical type of the DCCBs installed at both ends of the link34 are depicted in Fig. 10 (a). The primary protection was successful to interrupt the fault and the HVDC voltage comes back to the nominal value after some fluctuations. However, when the primary protection failed, the backup protection should act to interrupt the fault. The DC bus voltages when the fault is cleared by the MD-based backup protection are shown in Fig. 10 (b). although the DC voltage recovers to the operation state and the nominal value, it experiences larger and longer fluctuations compared to the case in Fig. 10 (a). Similar behavior can be seen from the measured load angle of the AC grid 2 in Fig. 11 for the cases of fault clearance by the MD-based primary and backup protections. However, the results of these cases show that the HVDC grid can keep its stability even under the long-time situation of fault interruption on the condition that the AC-connected grids are strong.

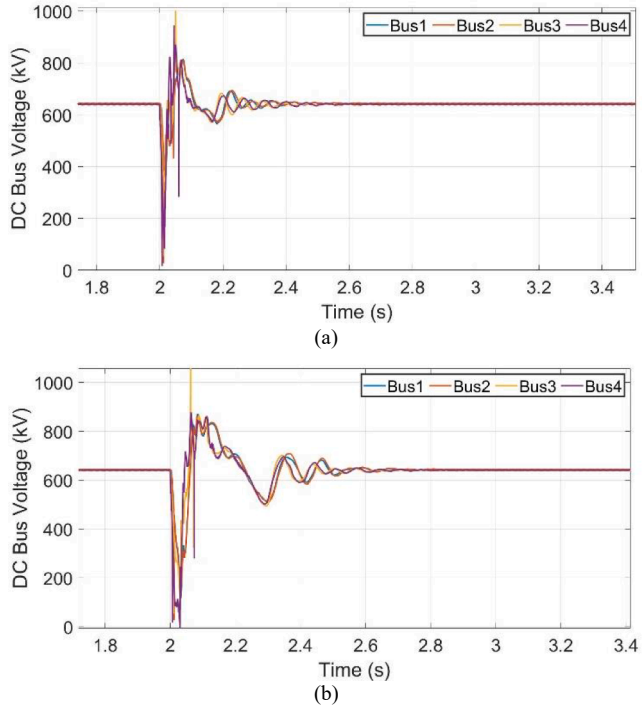

Fig. 10. DC bus voltages of the HVDC grid connected to strong AC grids during and after DC fault condition, (a) fault clearance by MD-based primary protection (b) fault clearance by MD-based backup protection.

5.2. The second case Study: Test results for the HVDC grid connected to a weak AC grid

For the second case study, the AC grid 2 is considered to be a weak grid with the SCR = 2.5. Fig. 12 and Fig. 13 depict the test results for this case. While the MD-based primary protection failed to secure the system against instability, the HB-based backup protection was successful to recover the HVDC voltage to the nominal value. In other words, if the hybrid type of the DCCBs is used, the system can keep its stability even if the primary protection failed. On the other hand, the results demonstrate that the DC protection design based on the mechanical DCCBs is not suitable for the HVDC system when it is connected to a weak AC grid.

To investigate the effect of the HVDC power value, the HVDC power received at the bus 4 and injected into the AC grid 2 has been increased by 400 MW. The results of this case are shown in Fig. 14 and Fig. 15. The HB-based backup protection cannot secure the HVDC system against instability anymore. However, the HB-based primary protection is still effective for the HVDC grid connected to the weak AC grid 2 with higher power absorption.

5.3. The third case Study: Test results for the HVDC grid connected to a very weak AC grid

For the third case study, the AC grid 2 is considered to be a very weak grid with the SCR = 2. Fig. 16 and Fig. 17 show the results of the DC bus voltages and the load angles respectively. Fig. 16 (a) shows that the HVDC voltage cannot recover to the nominal value if the HD-based backup protection must act to interrupt the fault. Moreover, the load angle instability can be seen from the results in Fig. 17 for the case of HD-based backup protection. However, the results demonstrate that the HD-based primary protection is effective to keep the system stable after fault clearance. Both the DC voltage and the load angle could recover to the nominal state when the primary protection based on the HDs was successful to interrupt the fault. Therefore, it is important to have

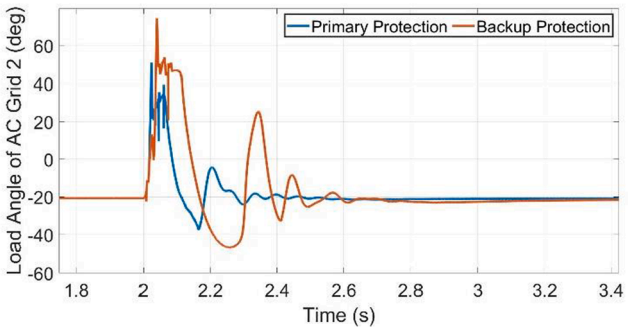

Fig. 11. Load angles of the strong AC grid 2 during and after DC fault clearance by MD-based primary and backup protections.

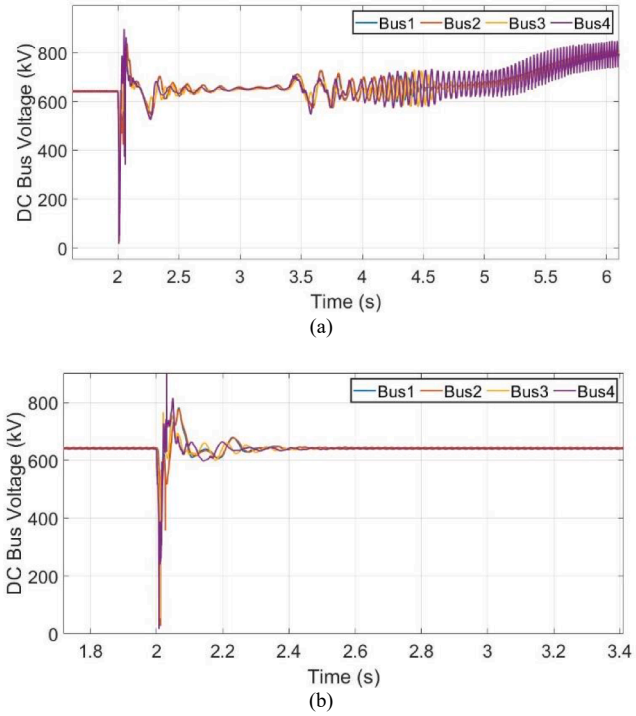

Fig. 12. DC bus voltages of the HVDC grid connected to weak AC grid 2 during and after DC fault condition, (a) fault clearance by MD-based primary protection (b) fault clearance by HD-based backup protection.

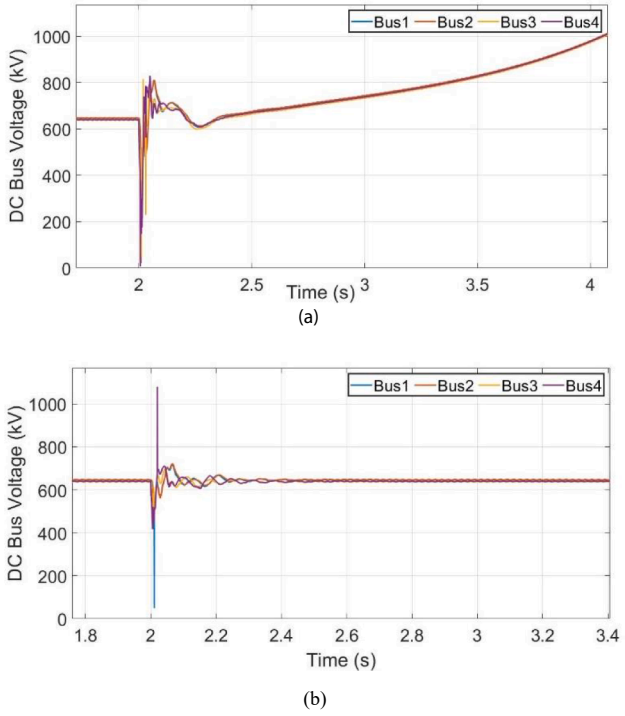

Fig. 14. DC bus voltages of the high-power HVDC grid connected to weak AC grid 2 during and after DC fault condition, (a) fault clearance by HD-based backup protection (b) fault clearance by HD-based primary protection.

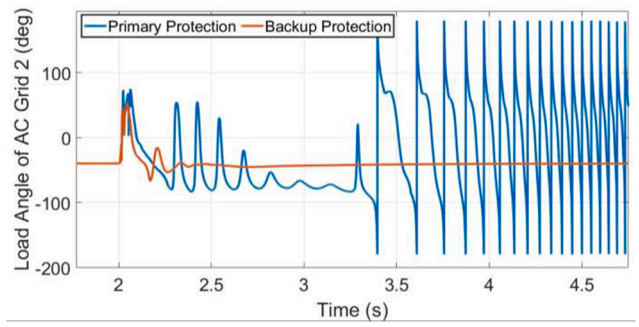

Fig. 13. Load angles of the weak AC grid 2 during and after DC fault clearance by MD-based primary protection and HD-based backup protection.

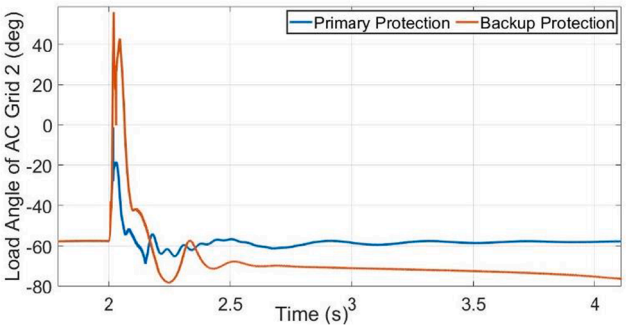

Fig. 15. Load angles of the weak AC grid 2 during and after DC fault clearance by HD-based primary protection and HD-based backup protection.

reliable primary protection based on the HDs when the system is connected to a very weak AC grid, as the backup protection is a risky solution in this case.

5.4. Test results for change in converter transformer Reactance, DC and arm inductances of the HVDC grid

To investigate the impacts of other system parameters including the leakage reactance of the converter transformer, DC and arm inductances, the simulations have been tested with different values of these parameters and the results are compared. The sizing of these inductances is usually based on a trade-off between many design parameters. However, their impact on the system's transient stability is investigated here. Fig. 18 shows the load angles of the weak AC grid 2 with different transformer reactances under DC fault conditions. While the load angle for the case with the transformer reactance of 0.1p.u. comes back to the nominal value after some small fluctuations, the case with the reactance of 0.15p.u experiences larger and longer fluctuations. However, the system could keep its stability for both of these cases. On the contrary, the system loses its stability for the case with the transformer reactance of 0.2 p.u. as depicted in Fig. 18. Therefore, larger transformer reactance may threaten the system's transient stability, which should be considered in the design of the HVDC grids

The impacts of the DC and arm inductances are analyzed and the results are depicted in Fig. 19 and Fig. 20. All signals of the load angles for the cases with different DC inductances of 0.1, 0.2 and 0.3H successfully converged and recovered to the initial value, as shown in Fig. 19. The cases with larger DC inductance face larger post-fault fluctuations and longer recovery time. On the other hand, the maximum load angles of the cases are shown in the zoomed part of Fig. 19. Although, the case with the largest DC inductance has the slowest response and recovery, it experiences the lowest value of the maximum load angle compared to other cases. The maximum load angle is directly related to the system's transient stability and the CCT [20]. The lower value of the maximum load angle corresponds to the lower risk of the system's instability. Thus, the larger DC inductance can improve the system's transient stability, as expected. However, it can make the system response and recovery slow.

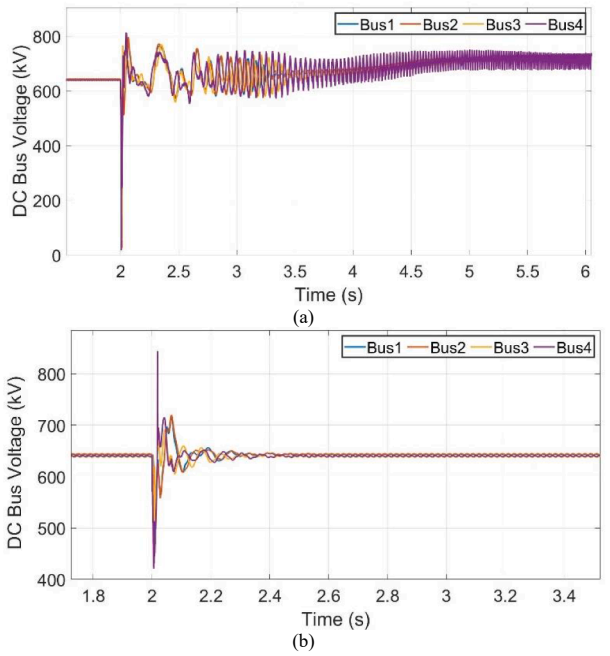

Fig. 16. DC bus voltages of the HVDC grid connected to very weak AC grid 2 during and after DC fault condition, (a) fault clearance by HD-based backup protection (b) fault clearance by HD-based primary protection.

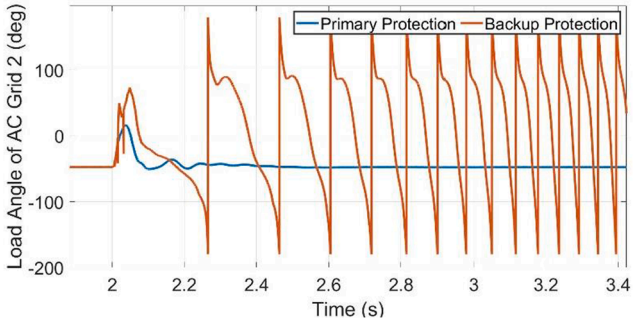

Fig. 17. Load angles of the very weak AC grid 2 during and after DC fault clearance by HD-based primary protection and HD-based backup protection.

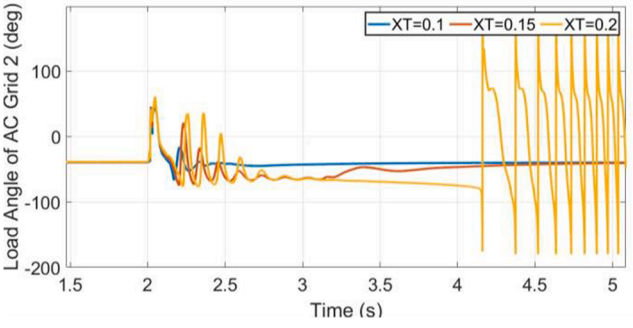

Fig. 18. Load angles of the weak AC grid 2 during and after DC fault clearance by HD-based backup protection with different transformer reactances.

The results for the cases with different arm inductances of 0.06, 0.16 and 0.26p.u. are depicted in Fig. 20. All signals successfully converged and recovered to the initial value after some fluctuations. However, the magnitude of the post-fault fluctuations and the maximum load angles are not the same. Not only the case with the largest arm inductance has the largest post-fault fluctuations but also has the highest value of the maximum load angle. Therefore, the larger arm inductance of the MMC converter can threaten the system's transient stability.

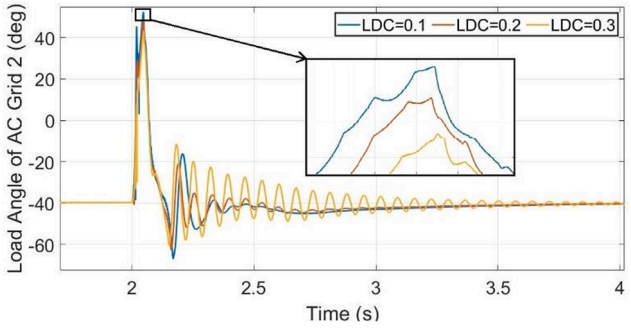

Fig. 19. Load angles of the weak AC grid 2 during and after DC fault clearance by HD-based backup protection with different DC inductances.

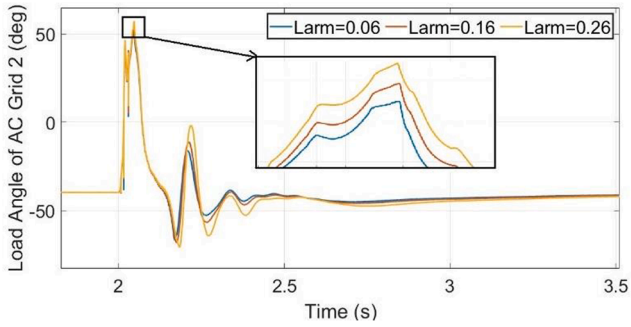

Fig. 20. Load angles of the weak AC grid 2 during and after DC fault clearance by HD-based backup protection with different arm inductances.

Table 1
DC Protection Parameters For The HVDC Test System.

DCCB Type	Parameters of DC Protection System				
	FDT	CDT	FITp	FITb	kSF
Hybrid	3 ms	2 ms	3 ms	3 ms	1.2
Mechanical	3 ms	2 ms	10 ms	10 ms	1.2

6. Conclusions

The study investigated the protection criteria of multi-terminal VSC-HVDC systems considering the transient stability of the embedded AC grid. At first, the analytic relations have been presented to analyze the impacts of the grid characteristics including SCR, HVDC power, the converter transformer reactance, DC and arm inductances on the system transient stability and CCT value. Then, a case study has been conducted to investigate the interactions between the DC protection and the transient stability responses. The simulation results showed that the DC protection based on the mechanical DCCBs is sufficient and reliable when the HVDC grid is connected to the strong AC grids. It can secure the system against instability and prevent high capital costs compared to the ones with the faster DCCBs. Consequently, it was not necessary to use a faster and overqualified DC protection, when the HVDC system was connected to the strong AC grids.

On the other hand, the results showed that while using the MD-based protection is risky for the HVDC grid connected to a weak AC grid, the HD-based protection is effective and reliable. Moreover, the backup protection based on the HDs could be effective when the primary protection failed to interrupt the DC fault. Also, it is necessary to use the

hybrid type of DCCBs for the HVDC system connected to a very weak AC grid. However, it is vital to make sure that the primary protection is highly reliable in this case, as the long performance time of the backup protection can threaten the system's stability. Furthermore, the results demonstrate that while the increase in the converter transformer and arm reactance can threaten the system's transient stability, an increase in DC inductance improves the transient stability. The study outcomes can be used for the DC protection design and transient stability analysis of the multi-terminal VSC-HVDC systems connected to strong and weak AC grids.

Declaration of competing interest

The authors declare that this work is supported by the Sino-Danish Center for Education and Research (SDC), University of Chinese Academy of Sciences.

Data availability

The data that has been used is confidential.

Appendix

References

[1] Reidy A, Watson R. Comparison of VSC based HVDC and HVAC interconnections to a large offshore wind farm. Meeting, San Francisco, CA: IEEE Power Eng. Soc. Gen; 2005.
[2] A. B. Morton, S. Cowdroy, J. R. A. Hill, M. Halliday, G. D. Nicholson, "AC or DC economics of grid connection design for offshore wind farms," Proc. IEEE Int. Conf. AC/DC Power Transm., pp. 236-240, 2006.
[3] Wang M, An T, Ergun H, Lan Y, Andersen B, Szechtman M, et al. Review and outlook of HVDC grids as the backbone of the transmission system. CSEE J Power Energy Syst 2020.
[4] Wang WY, Barnes M. Power flow algorithms for Multi-terminal VSC-HVDC with droop control. IEEE Trans Power Syst 2014;29(4):1721–30.
[5] Deng F, Chen Z. Operation and Control of a DC-Grid Offshore Wind Farm under DC Transmission System Faults. IEEE Trans Power Delivery 2013;28(3):pp.
[6] Shu H, Wang G, Tian X, et al. Single-ended protection method of MMC-HVDC transmission line based on random matrix theory. Int J Electr Power Energy Syst 2022;142:108299.
[7] Nadeem MH, Zheng X, Tai N, et al. Non-communication based protection scheme using transient harmonics for multi-terminal HVDC networks. Int J Electr Power Energy Syst 2021;127:106636.
[8] Zhao Z, Lan T, Xiao H, et al. Wave front rising time based traveling wave protection for multi-terminal VSC-HVDC grids. Int J Electr Power Energy Syst 2023;144: 108534.
[9] Zhang Y, Wei C. An improved single-ended frequency-domain-based fault detection scheme for MMC-HVDC transmission lines. Int J Electr Power Energy Syst 2021; 125:106463.
[10] Wang Y, Yuan Z, Fu J, et al. A feasible coordination protection strategy for MMC-MTDC systems under dc faults. Int J Electr Power Energy Syst 2017;90:103–11.
[11] S. H. Ashrafi Niaki, Z. Liu, Z. Chen, B. Bak-Jensen, and S. Hu, "Protection System of Multi-Terminal MMC-based HVDC grids: A Survey," the 6th International Conference on Power Energy Systems and Applications (ICoPESA), 2022.
[12] Yu X, Gu J, Zhang X, Mao J, Xiao L. A self-adaptation non-unit protection scheme for MMC-HVDC grids based on the estimated fault resistance. Int J Electr Power Energy Syst 2023;152:109263.
[13] Li B, Li Y, Li B, Chen X, Ji L, Hong Q. A Non-unit transient travelling wave protection scheme for multi-terminal HVDC system. Int J Electr Power Energy Syst 2023;152:109263.
[14] Meegahapola L, Sguarezi A, Bryantet JS, Gu M, Conde ER, Cunha RBA. Power System Stability with Power-Electronic Converter Interfaced Renewable Power Generation Present Issues and Future Trends. Energies 2020;13(13):1–35.
[15] C. Liu, Z. Chen, C. L. Bak, Z. Liu, P. Lund, P. Rønne-Hansen, "Transient Stability Assessment of Power System with Large Amount of Wind Power Penetration the Danish Case Study," 10th International Power & Energy Conference (IPEC), 2012.
[16] Abedrabbo M, Wang M, Tielens P, Dejene FZ, Leterme W, Beerten J, et al. "Impact of DC grid contingencies on AC system stability. 13th IET International Conference on AC and DC Power Transmission (ACDC 2017), Manchester, UK. 2017.
[17] W. Leterme, D. V. Hertem, "Classification of Fault Clearing Strategies for HVDC Grids," Cigre, 21, rue d'Artois, Paris, 2015.
[18] B. Li, A. Li, W. Wen, B. Li, X. Chen, Q. Hong, L. Ji, "A protection scheme for MMC–HVDC grid based on blocking time of converter station, vol. 152, 109263, 2023.
[19] Barnes M, Vilchis-Rodriguez DS, Pei X, Shuttleworth R, Cwikowski O, Smith AC. HVDC Circuit Breakers–A Review. IEEE Access 2020;8:211829–48.
[20] Kundur P. Power System Stability and Control. New York: McGraw-Hill; 1994.
[21] Yang J, Fletcher JE, O'Reilly J. Multi-terminal DC wind farm collection grid internal fault analysis and protection scheme design. IEEE Trans Power Delivery 2010;25(4):2308–18.
[22] Nagrath DPK. Modern Power System Analysis. second edition. McGraw-Hill; 2001.
[23] PROMOTioN project,. Requirement recommendations to adapt and extend existing grid codes. Deliverable 2020;2:4.
[24] S. H. Ashrafi Niaki, Z. Chen, B. Bak-Jensen, K. Sharifabadi, Z. Liu and S. Hu, "On Systematic DC Fault-Ride-Through of Multi-terminal MMC-HVDC Grids," 2021 56th International Universities Power Engineering Conference (UPEC), 2021.
[25] W. Leterme, S. Pirooz Azad and D. Van Hertem, "A Local Backup Protection Algorithm for HVDC Grids," in IEEE Transactions on Power Delivery, vol. 31, no. 4, pp. 1767-1775, Aug. 2016.
[26] PROMOTIONOTIOM project, "Progress on Meshed HVDC Offshore Transmission Networks," D9.3, Selective protection system demonstration, 2020.
[27] Franck CM. HVDC Circuit Breakers: A Review Identifying Future Research Needs. IEEE Trans Power Delivery 2011;26(2):998–1007.
[28] W. Leterme, N. Ahmed, J. Beerten, L. Ängquist, D. V. Hertem and S. Norrga, "A new HVDC grid test system for HVDC grid dynamics and protection studies in EMT-type software," 11th IET International Conference on AC and DC Power Transmission, 2015.